

PAPER

Pick-and-place process for sensitivity improvement of the capacitive type CMOS MEMS 2-axis tilt sensor

To cite this article: Chun-I Chang *et al* 2013 *J. Micromech. Microeng.* **23** 095029

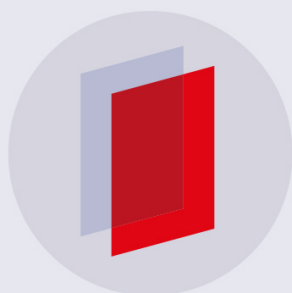
View the [article online](#) for updates and enhancements.

Related content

- [Design and application of a metal wet-etching post-process for the improvement of CMOS-MEMS capacitive sensors](#)
Ming-Han Tsai, Chih-Ming Sun, Yu-Chia Liu *et al.*
- [Post-CMOS selective electroplating technique for the improvement of CMOS-MEMS accelerometers](#)
Yu-Chia Liu, Ming-Han Tsai, Tsung-Lin Tang *et al.*
- [Development of CMOS-MEMS in-plane magnetic coils for application as a three-axis resonant magnetic sensor](#)
Chun-I Chang, Ming-Han Tsai, Chih-Ming Sun *et al.*

Recent citations

- [Three-Dimensional Anisotropic Metamaterials as Triaxial Optical Inclinometers](#)
Kriti Agarwal *et al*
- [A low-temperature ZnO nanowire ethanol gas sensor prepared on plastic substrate](#)
Chih-Hung Lin *et al*
- [Development of a large-area chip network with multidevice integration using a stretchable electroplated copper spring](#)
Wei-Lun Sung *et al*



IOP | ebooks™

Bringing you innovative digital publishing with leading voices to create your essential collection of books in STEM research.

Start exploring the collection - download the first chapter of every title for free.

Pick-and-place process for sensitivity improvement of the capacitive type CMOS MEMS 2-axis tilt sensor

Chun-I Chang¹, Ming-Han Tsai², Yu-Chia Liu¹, Chih-Ming Sun²
and Weileun Fang^{1,3}

¹ Institute of NanoEngineering and MicroSystems, National Tsing Hua University, Hsinchu, Taiwan

² PixArt Imaging Inc., Hsinchu, Taiwan

³ Power Mechanical Engineering, National Tsing Hua University, Hsinchu, Taiwan

E-mail: fang@pme.nthu.edu.tw

Received 19 April 2013, in final form 18 July 2013

Published 28 August 2013

Online at stacks.iop.org/JMM/23/095029

Abstract

This study exploits the foundry available complimentary metal-oxide-semiconductor (CMOS) process and the packaging house available pick-and-place technology to implement a capacitive type micromachined 2-axis tilt sensor. The suspended micro mechanical structures such as the spring, stage and sensing electrodes are fabricated using the CMOS microelectromechanical systems (MEMS) processes. A bulk block is assembled onto the suspended stage by pick-and-place technology to increase the proof-mass of the tilt sensor. The low temperature UV-glue dispensing and curing processes are employed to bond the block onto the stage. Thus, the sensitivity of the CMOS MEMS capacitive type 2-axis tilt sensor is significantly improved. In application, this study successfully demonstrates the bonding of a bulk solder ball of 100 μm in diameter with a 2-axis tilt sensor fabricated using the standard TSMC 0.35 μm 2P4M CMOS process. Measurements show the sensitivities of the 2-axis tilt sensor are increased for 2.06-fold (x -axis) and 1.78-fold (y -axis) after adding the solder ball. Note that the sensitivity can be further improved by reducing the parasitic capacitance and the mismatch of sensing electrodes caused by the solder ball.

(Some figures may appear in colour only in the online journal)

1. Introduction

The tilt sensor has been extensively employed in many applications, such as in the automobile industry, consumer electronics, navigation systems, and robotics [1]. The micromachining technology is considered a promising approach to bring various advantages for tilt sensors, such as size and cost reduction. Presently, various micromachined tilt sensors have been reported, such as the electrolytic-based [2], gas-filled [3–5], and liquid metal [6] designs. These devices successfully demonstrate the small size tilt sensors, yet many issues still cannot be ignored. The electrolytic-based tilt sensor in [2] has challenging fabrication processes and the reliability issue. The gas-filled tilt sensors based on thermal convection in [3] has small linear range and its performance is sensitive to environment temperature. Moreover, the materials such as

mercury and galinstan for the liquid metal tilt sensor [6] have the problems of toxic and oxidation issues [7]. Comparing with the existing heat convection or electrolyte sensing approaches, the capacitive detection method has been highlighted due to its low power consumption, long lifetime, and reduced sensitivity to the surrounding temperature. Thus, the capacitive type tilt sensors consisted of spring-mass structure have been reported in [8, 9]. As discussed in [8], the wafer bonding technology has been employed to implement the capacitive type tilt sensor. The quartz-based microelectromechanical systems (MEMS) capacitive tilt sensor in [9] has the advantages of high sensitivity and low-noise, but its process is relatively complicated.

The mature complimentary metal-oxide-semiconductor (CMOS) processes have recently been implemented in various MEMS sensing devices [10–13]. The CMOS MEMS

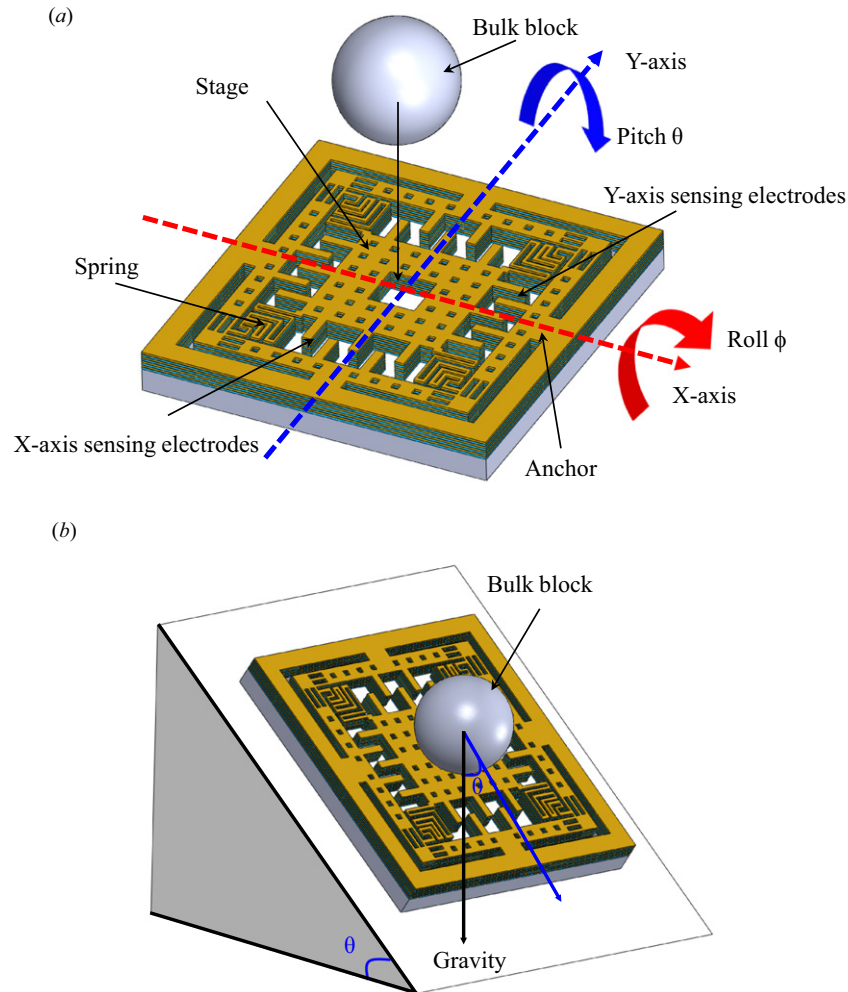


Figure 1. Schematic of the proposed CMOS MEMS tilt sensor (a) the spring, stage, and sensing electrodes are formed by thin films, and (b) the bulk block is bonded onto the stage to enhance the proof-mass.

technology enables the monolithic integration of integrated circuits (IC) and MEMS components, so as to reduce the parasitic capacitance of capacitive sensing devices. On the other hand, the designs of mechanical components are limited to the available thin film layers for standard CMOS processes. For example, the sensitivity of CMOS MEMS accelerometer is limited by the proof-mass [14]. Various approaches have been investigated to improve the performance of CMOS MEMS capacitive sensors [15, 16]. For instance, the sensitivity can be enhanced by increasing the number of sensing electrodes [15], and by reducing the size of sensing gap [16]. The sensitivity of various sensors can be further improved by increasing their proof-mass [17, 18]. The backside through-wafer Si etching has also been exploited to increase the proof-mass and sensitivity of CMOS MEMS sensors [17]. The post-CMOS selective Ni electroplating technology has also been employed to improve the proof-mass of the CMOS MEMS accelerometers [18].

The pick-and-place is a mature technology for packaging. Pick-and-place technology has also been exploited to assemble MEMS structures using the micromachined gripper [19–21]. This study exploits the pick-and-place technology to assemble a lump mass onto the micromachined structure so as to

increase the proof-mass of the CMOS MEMS sensors. Thus, the additional fabrication processes such as the backside etching and Ni electroplating in [17, 18] are not required. In application, a 2-axis capacitive type tilt sensor is designed and implemented using the standard CMOS plus the post-CMOS processes. After that, the bulk solder ball is assembled onto the 2-axis tilt sensor using the pick-and-place approach to increase its proof-mass and sensitivity. This approach has been exploited to improve the performance of 1-axis capacitive type tilt sensor in [22]. During the pick-and-place process, a low temperature UV-glue dispensing and curing process is established to bond the bulk solder ball on a suspended stage. Such simple post-CMOS process inherited from the mature technology for packaging provides an easy approach to improve the performance of CMOS MEMS sensors.

2. Design concept

Figure 1 shows the schematic design of the present 2-axis tilt sensor. As shown in figure 1(a), the micro fabricated sensing chip consists of suspended springs, a stage (with a center alignment hole), and sensing electrodes. An additional bulk block is mounted onto the suspended stage to form the

proof-mass of the tilt sensor. Note the standard TSMC 0.35 μm 2P4M (two poly-Si and four metal layers) CMOS foundry process and in-house post-CMOS process are employed to implement the suspended micromachined structures on chip. The bulk block is placed onto the stage using the pick-place process. A low temperature glue (UV curable) dispensing and curing process is further established to bond the bulk block on such suspended micromachined stage. In this regard, the alignment hole on stage is designed to ease the assembly and bonding of the bulk block. The design of presented 2-axis tilt sensor enables the detection of the tilt angles of pitch (θ_{tilt} , tilt about y -axis) and roll (ϕ_{tilt} , tilt about x -axis), as indicated in figure 1(a). Note the gravitational force G is in the z -axis. The folded springs are designed to be flexible in the two in-plane axes (x -axis and y -axis). As the sensor tilted with θ_{tilt} (or ϕ_{tilt}) in figure 1(b), the gravitational force $G \sin \theta_{\text{tilt}}$ (or $G \sin \phi_{\text{tilt}}$) will cause the in-plane displacement of proof-mass and further lead to the gap variation between sensing electrodes. Thus, the in-plane displacement of proof-mass as well as the tilt angle (θ_{tilt} or ϕ_{tilt}) of chip is determined by the measured output signal. Moreover, the fully differential sensing electrodes and their sensing circuits are also implemented and integrated using the same standard CMOS process. The preamplifier in this study acted as a buffer with a gain (Gain_{amp}) of one. According to [23], the output voltage of the presented tilt sensor V_{out} can be predicted as,

$$V_{\text{out}} = \frac{mG \sin \theta_{\text{tilt}}}{K} \times \frac{C_0}{g_0} \times \frac{4V_m}{(C_p + 2C_0)} \times \text{Gain}_{\text{amp}} \quad (1)$$

where M and K are the proof-mass and spring constant of the tilt sensor, C_0 is the initial capacitance for all sensing electrodes, g_0 is the initial sensing gap between the fixed and movable comb-finger electrodes, C_p is the parasitic capacitance and V_m is the input modulation voltage. The proof-mass is mainly contributed from the stage of mass m_s before adding the bulk block indicated in figure 1. Thus, the sensitivity can be easily and significantly improved by adding the bulk block of mass m_b , and the proof-mass becomes $M = m_s + m_b$. Note that according to [5], the sensitivity of tilt sensor is determined by the slope of the measured V_{out} versus tilt angle (θ_{tilt} or ϕ_{tilt}) with a range between 0° to 30° .

In general, the stage consisted of the stacked thin metal-dielectric layers of CMOS process, has a mass m_s in the order of micrograms. According to equation (1), the sensitivity of the tilt sensor will be influenced by proof-mass M . This study employs the commercial available solder ball with relatively large mass m_b as the bulk block. The diameter D and mass m_b of the solder ball employed in this study are $100 \mu\text{m}$ and $3.87 \mu\text{g}$, respectively. Moreover, the planar dimension of the micromachined stage is $300 \mu\text{m} \times 300 \mu\text{m}$ with an alignment hole of $55 \mu\text{m} \times 55 \mu\text{m}$ at its center. Hence, the mass of stage is $m_s = 1.47 \mu\text{g}$. The sensing gap is designed to be the minimum width of metal layers ($0.8 \mu\text{m}$) to increase the capacitance change. Table 1 summarizes the typical design values of the presented 2-axis capacitive tilt sensor with different size solder balls. According to the dimensions and gap of sensing electrodes, the initial sensing capacitance of the x -axis sensing electrodes as well as the y -axis sensing electrodes is $C_0 = 58.5 \text{ fF}$. Moreover, based on

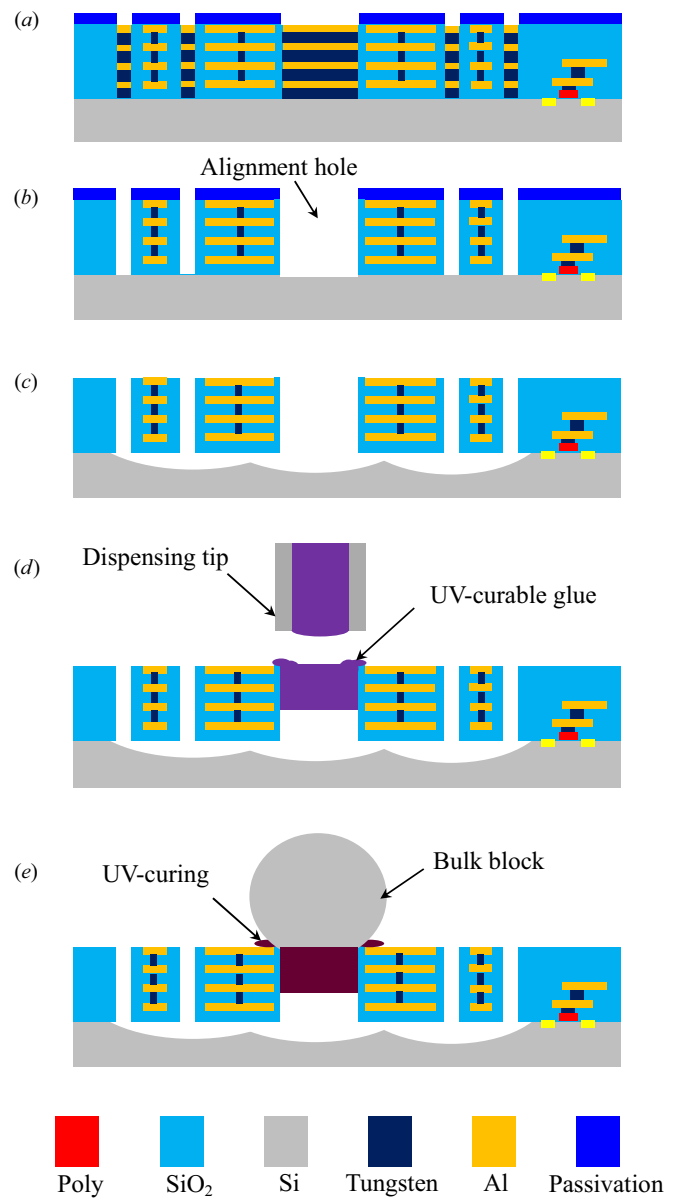


Figure 2. The fabrication process steps, (a) the thin films stacking and patterning after the standard TSMC 0.35 μm CMOS process, (b) the metal wet etching, (c) the XeF₂ bulk Si isotropic etching, (d) the UV-curable glue dispensing, and (e) the pick-and-place of bulk block and then bonding to the stage after UV-curing.

the design of electrical routings, the parasitic capacitance of the tilt sensor with no bulk solder ball is estimated as $C_p = 500 \text{ fF}$ [18]. As the input modulation voltage (V_m) is 1V, the corresponding x -axis sensitivity determined from equation (1) is 2.6 mV/degree (without bulk solder ball), 8.4 mV/degree (with $100 \mu\text{m}$ bulk solder ball), respectively. The y -axis sensitivity determined from equation (1) is 3.2 mV/degree (without bulk solder ball), 10.3 mV/degree (with bulk solder ball of $D = 100 \mu\text{m}$) respectively. Simulation results also indicate that the monolithic integrated ICs having 10 MHz bandwidth and 4.3 mW power dissipation. In summary, the standard CMOS process and the in-house post-CMOS process are exploited to implement the tilt sensor and its sensing circuits. The mature pick-and-place technique for the

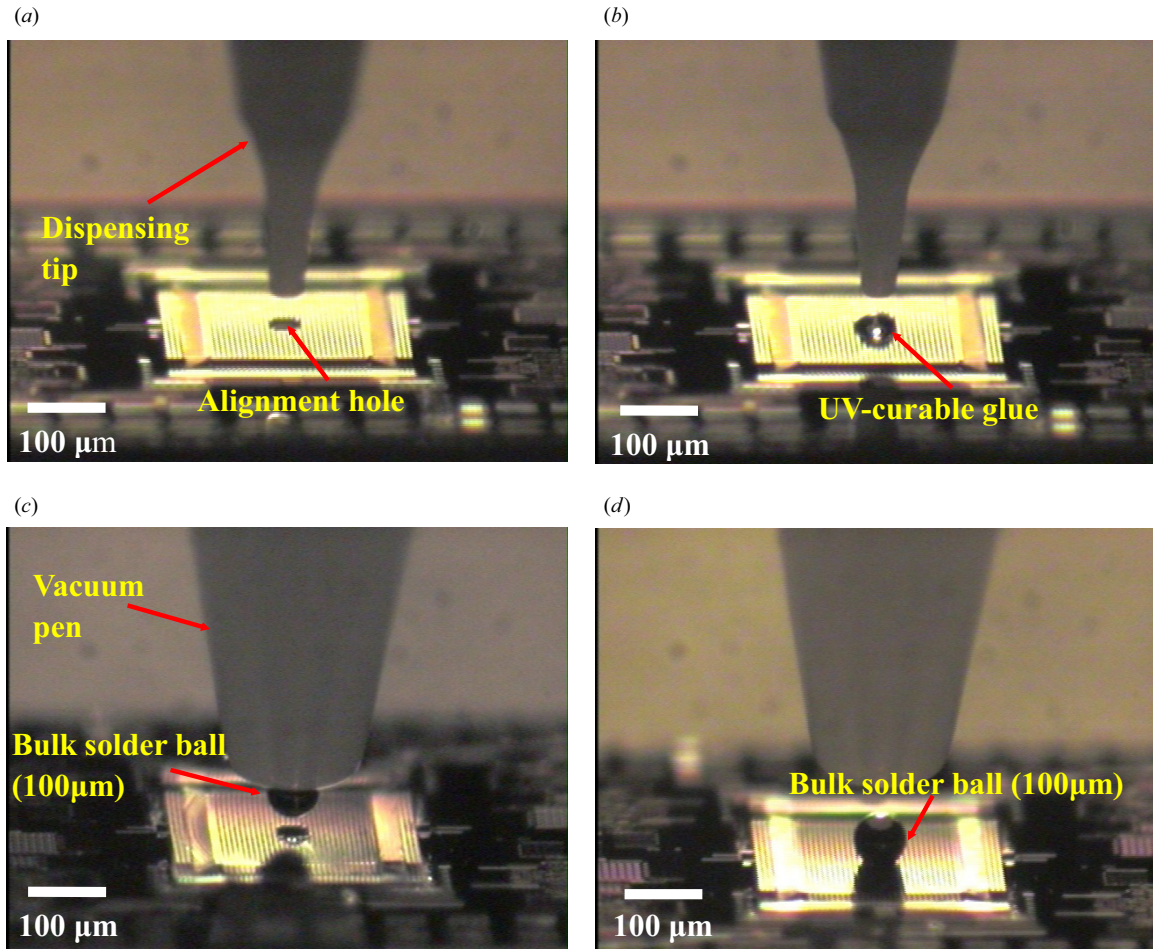


Figure 3. The optical micrographs of, (a)–(b) the UV-glue dispensing on the alignment hole of stage, and (c) positioning of the bulk solder ball (100 μm in diameter) on the alignment hole of stage by pick-and-place process, and (d) adhering of the solder ball on stage after UV-curing.

Table 1. The design vales of the 2-axis capacitive type tilt sensor.

Parameters	Design specifications of the tilt sensor	
	Without bulk solder ball	With bulk solder ball (100 μm)
Proof-mass size	300 \times 300 μm^2	
Weight of Proof-mass	1.47 μg	5.34 μg
Sensing finger gap (g_0)	0.8 μm	0.8 μm
Length of the sensing finger	50 μm	50 μm
x-axis spring stiffness	10.97 N/m	10.97 N/m
y-axis spring stiffness	8.94 N/m	8.94 N/m
z-axis spring stiffness	14.4 N/m	14.4 N/m
Initial capacitance (C_0)	58.5 fF	58.5 fF
x-axis Sensitivity	2.6 mV/degree	8.4 mV/degree
y-axis Sensitivity	3.2 mV/degree	10.3 mV/degree

packaging house is further employed to add bulk solder balls of different sizes onto the tilt sensor to change its proof-mass. Thus, the sensitivity as well as sensing range of the CMOS MEMS tilt sensor can be easily modulated by using the pick-and-place technique. As limited by the films stacking of standard CMOS process, the MEMS structures in this study has a maximum thickness of 6.97 μm . Thus, the out-of-plane to in-plane stiffness ratio for the presented spring design is only

1.3 for z-axis/x-axis and 1.6 for z-axis/y-axis, as summarized in table 1. The out-of-plane deformation of the springs due to the loading of bulk solder ball cannot be ignored. As a result, the net overlap area of the sensing electrodes as well as the sensing capacitance will be reduced. This problem needs to be considered to improve the design.

3. Fabrication and results

This study has established the fabrication processes in figure 2 to implement the presented tilt sensor. As shown in figure 2(a), the chip was first fabricated using the standard TSMC 0.35 μm 2P4M CMOS foundry process. The thin films were patterned based on our layout design, and the wet etching windows were defined by the passivation layer. As illustrated in figure 2(b), the metal wet etching process was employed to define the planar shape of the MEMS structure, the alignment hole for bulk block and the sensing gaps. The passivation layer was then removed by reactive ion etching to expose the bond pads. After that, the substrate was etched isotropically using the XeF_2 to suspend the MEMS structures, as shown in figure 2(c). As depicted in figure 2(d), the UV-curable glue was then precisely dispensed into the alignment hole using a commercial pneumatic dispensing system. The alignment hole

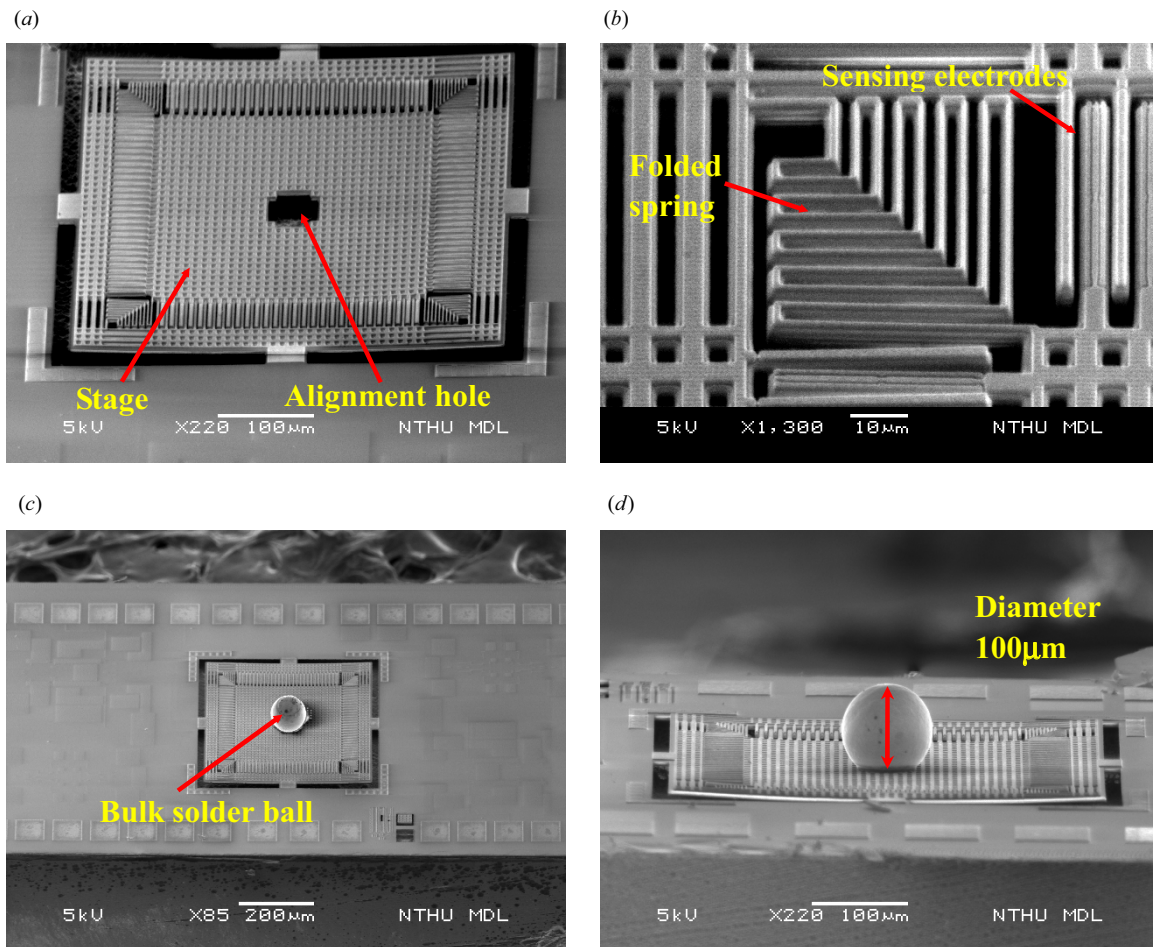


Figure 4. The SEM micrographs of typical fabrication results, (a) the suspended stage with no bulk solder ball, (b) the zoom-in micrograph showing the spring and sensing electrodes, and (c)–(d) the tilt sensor with a bulk solder ball of 100 μm in diameter.

is also exploited to trap the glue to prevent it from spreading to the stage. The commercial pneumatic dispensing system could provide a minimum dispensing volume of 0.03 nl with a volume deviation of $\pm 1.3\%$. The NOA63 (Norland Optical Adhesive Inc., USA) was selected as the UV-curable glue. The bulk block was picked by the vacuum pen and then placed on the alignment hole by micro-manipulator. As shown in figure 2(e), the solder ball was fixed to the stage by glue after the UV curing process. The commercial solder ball (Accurus Scientific Co., Ltd) with diameter of 100 μm was selected as the bulk block.

In applications, the 2-axis CMOS MEMS tilt sensors with bulk solder ball were successfully implemented using the processes in figure 2. The photographs in figure 3 show different steps of the processes. As shown in figures 3(a), (b), the liquid UV-curable glue is dispensed into the alignment hole of 55 $\mu\text{m} \times 55 \mu\text{m}$, and the volume of glue is precisely controlled by the pneumatic dispensing system. Note the dispensing tip (Kulicke and Soffa Industries, Inc.) has an inner diameter of 30 μm . The photograph also indicates the glue is properly trapped inside the alignment hole. The photograph in figure 3(c) shows a solder ball of $D = 100 \mu\text{m}$ picked by a vacuum pen. The photograph in figure 3(d) further display the solder ball placed inside the alignment hole by

a micro manipulator. After that, the liquid UV-curable glue is solidified by UV light. It demonstrates the proof-mass of the tilt sensors can be changed by using the pick-and-place of bulk solder balls, hence no masks and micro fabrication processes are required. The scanning electron microscopy (SEM) micrographs in figure 4 show the typical fabrication results. Figure 4(a) shows the suspended stage with no bulk solder ball attached. The alignment hole is thus observed. The zoomed-in micrograph in figure 4(b) displays the spring and sensing electrodes. Figures 4(c), (d) show the tilt sensor with a bulk solder ball of $D = 100 \mu\text{m}$. Note that the sensing circuit indicated in the SEM micrograph is also embedded inside the chip.

4. Testing and results

Various tests have been performed to characterize the performance of the fabricated tilt sensor. Firstly, the surface profile of the tilt sensor (before and after adding bulk solder ball) has been measured to characterize the initial deformation of suspended structures and the initial offset of sensing electrodes. Figure 5 displays the typical measured surface profiles of sensing electrodes for the tilt sensor using a commercial optical interferometer (Veeco Inc., NT-1100).

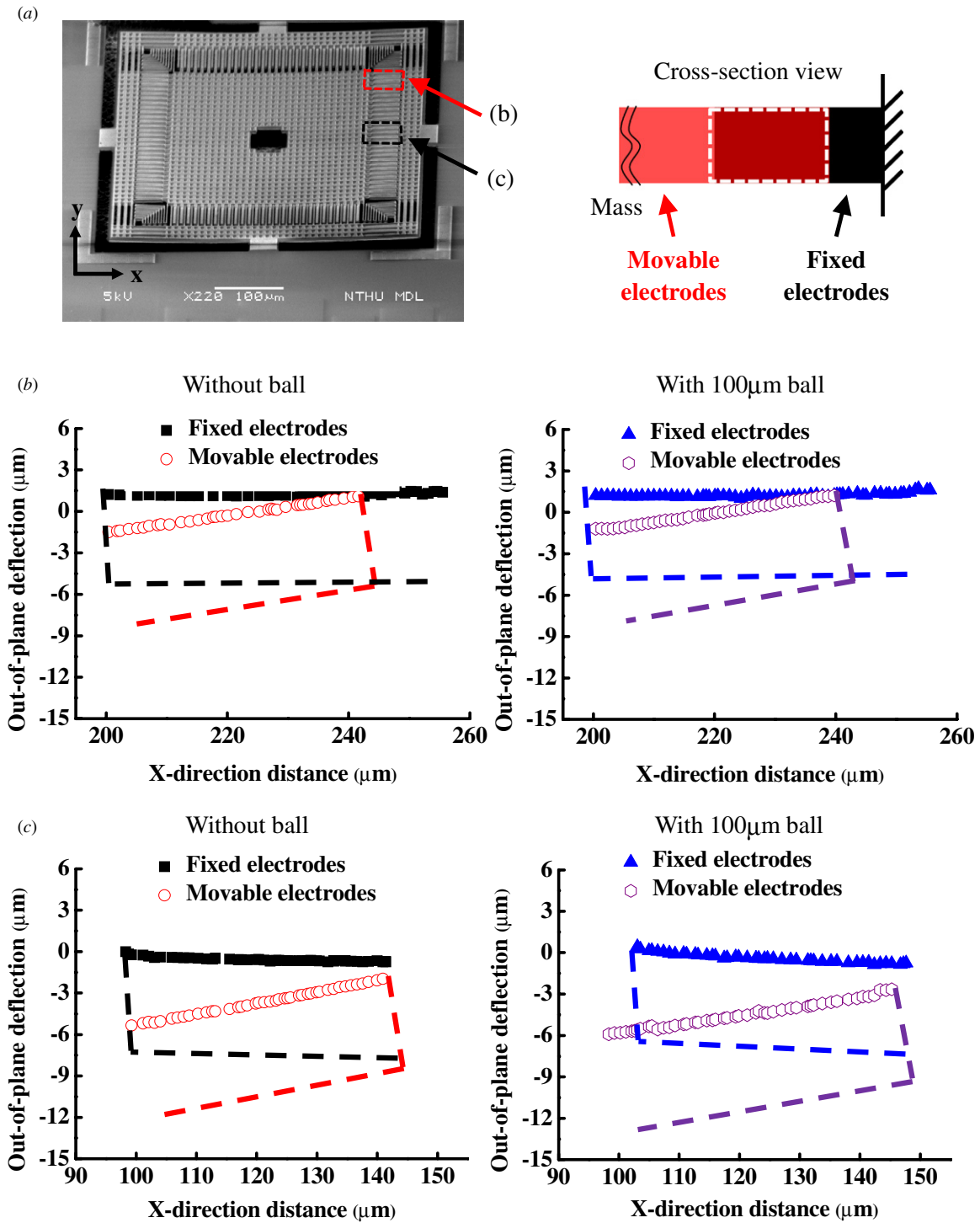


Figure 5. The typical measured surface profiles of sensing electrodes for tilt sensor, (a) the SEM micrograph showing the locations of the sensing electrodes measured in this figure, and (b)–(c) respectively show the measured surface profiles (solid lines) of fixed/movable electrodes at the positions indicated in (a), and the dashed lines show the shape of sensing electrodes.

As the SEM micrograph depicted in figure 5(a), the y-axis sensing electrodes at the edge and the center of stage are measured. In addition, the idea overlap sensing area indicated in figure 5(a) is designed to be $8490 \mu\text{m}^2$. The solid lines in figures 5(b), (c) show the measured surface profiles of fixed/movable electrodes at the positions indicated in figure 5(a). The dashed lines have been illustrated in figures 5(b), (c) to indicate the positions of fixed/movable

sensing electrodes. Typical measurements show the overlap area of fixed and movable sensing electrodes becomes $5700 \mu\text{m}^2$ after the bi-axial bending by thin film residual stresses. The typical overlap area of sensing electrodes after the out-of-plane deformation/displacement of stage by the weight of solder ball becomes $5250 \mu\text{m}^2$.

The optical micrographs in figure 6 display the chips after wire bonding for the following functional tests. In

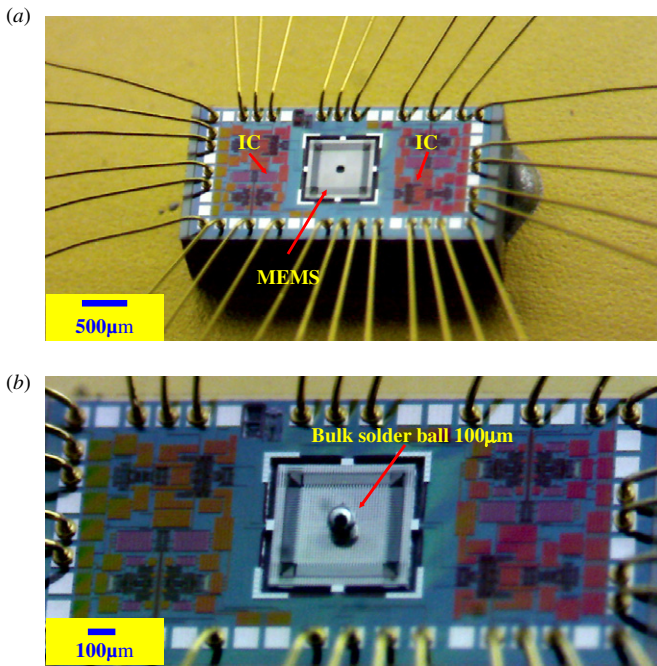


Figure 6. The optical micrographs show the monolithic integration of sensing circuits and the mechanical components for the presented CMOS MEMS tilt sensor after packaging, (a) tilt sensor without bulk solder ball, and (b) tilt sensor with the bulk solder ball of 100 μm in diameter.

this study, the sensing circuits and electrical routings are mainly covered with the silicon dioxide films as shown in figure 2. Thus, the sensing circuits and electrical routings are observed in these micrographs since the silicon dioxide films are transparent under optical microscopy. The micrographs indicate the MEMS structures, solder balls of different sizes (100 μm) and sensing circuits are monolithically integrated in the same chip. Figure 7 shows the experiment setup for the performance test of tilt sensor. The tilt sensor is mounted on a commercial rate table (Acutronic Inc., AC1120S) to control the tilt angle. The modulation signals (1 Vp-p. at 1 MHz) provided by the function generator was input to tilt sensor during the measurement. The capacitance change induced by the variation of tilt angle was characterized by the output dc-level of the modulation signal using a multi-meter (Keithley Inc., Model-2700). Figure 8 shows the typical measured sensing voltages versus tilt angles. Figure 8(a) shows the data with a tilt angle from 0° to 90°, and the sine curve voltage change can be observed. The dashed lines are simulated sine curves for reference. Moreover, the sensitivity of a tilt sensor is determined by the linear slope of the measured V_{out} versus tilt angle (θ_{tilt} or ϕ_{tilt}) within a range between 0° to 30° according to [5], as indicated in figure 8(b). In comparison, this study performed the measurements on tilt sensors with and without bulk solder ball. The measurements in figure 8(b) are detected using the tilt sensor with bulk solder ball of 100 μm diameter. The measurement results in figure 8(b) indicate the x -axis sensitivity of tilt sensor is increased from 2.01 to 4.15 mV/degree after adding the 100 μm solder ball. Moreover, the y -axis sensitivity of the same tilt sensor is increased from 2.65 to 4.71 mV/degree after adding the

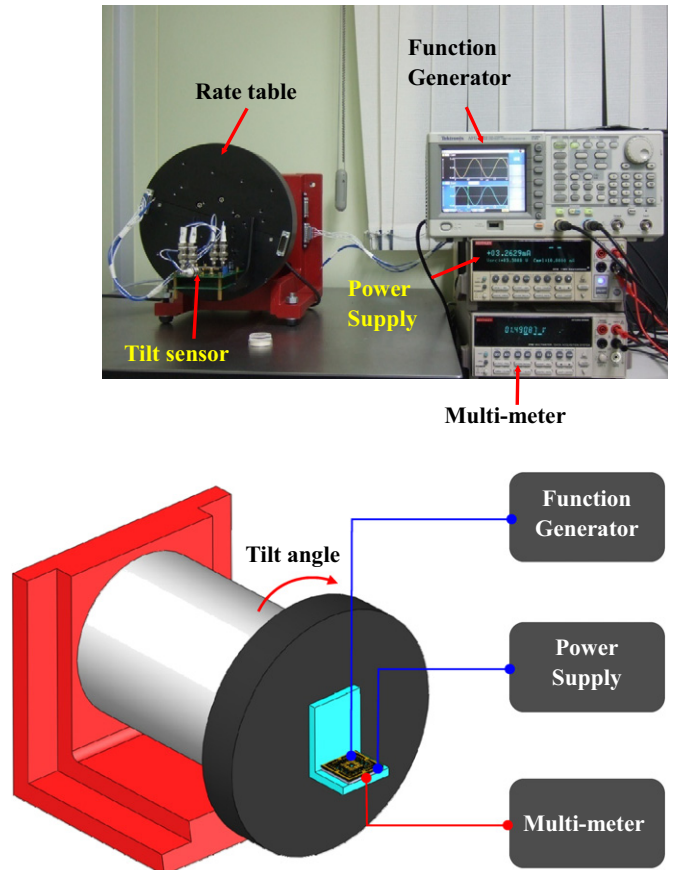


Figure 7. The photo and schematic illustration of the test setup for the characterization of tilt sensor.

solder ball. As a result, the sensitivities of the tilt sensor have been increased for 2.06-fold (in x -axis) and 1.78-fold (in y -axis), after adding the 100 μm solder ball (i.e. proof-mass M increased from 1.47 to 5.34 μg). The noise measurement results are shown below. In this study, the noise floor of x -axis is 0.129 mV/rHz (after adding solder ball), and y -axis is 0.136 mV/rHz (after adding the solder ball). In comparison, the noise floor of the tilt sensor in [22] is 0.0495 mV/rHz. The same sensing circuits have been employed to convert capacitance to voltage for the sensors in this study and [22]. It indicates that the Brownian noise could be reduced by increasing the proof-mass after adding the bulk solder ball. In short, the low temperature pick-and-place assembly/bonding technology can be exploited to improve the capacitive type tilt sensor fabricated using the standard TSMC 0.35 μm 2P4M CMOS process.

According to equation (1), the ideal sensitivity enhancement after adding the 100 μm solder ball should be 3.63-fold for both the x -axis and y -axis. Measurements indicate the bulk solder ball did increase the sensitivity of the CMOS MEMS tilt sensor, however the sensitivity enhancement is smaller than the predicted one. There are several reasons as to why the measured sensitivity is smaller than the predicted one. First, as indicated in figure 5, the MEMS stage is deformed by the weight of the solder ball and further lead to the overlap area decrease (near 10%) of sensing electrodes. Thus, the sensing signal is also decreased by nearly 10%.

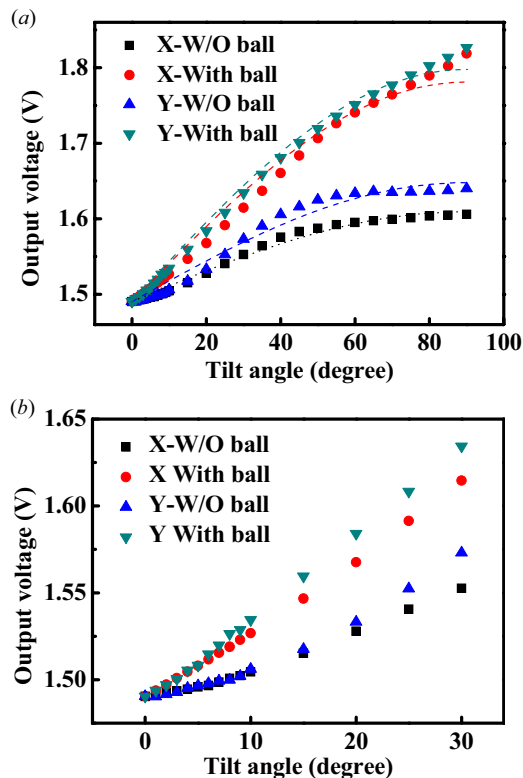


Figure 8. Characterization of the output voltages versus tilt angles for tilt sensor with and without solder ball ($100\ \mu\text{m}$ in diameter), and the measurement range of (a) tilt angles is 0° – 90° , and (b) tilt angles is 0° – 30° .

Second, the measured solder ball diameter is $96\ \mu\text{m}$ but not the designed value of $100\ \mu\text{m}$. The 4% decreasing of solder ball diameter will introduce a 12% reduction of its volume as well as mass. Third, the solder ball will lead to an additional parasitic capacitance to the sensor, and then decrease the sensing signal. According to the simulation by commercial software (CoventorWare), the bulk solder ball will lead to an additional parasitic capacitance of 80 fF. After considering the above three effects, the sensitivity enhancement determined from equation (1) becomes 2.31-fold for both x -axis and y -axis. Thus, the measured sensitivity enhancement is still $\sim 11\%$ below the predicted one for x -axis, and $\sim 23\%$ below the predicted one for y -axis. Further study is still required to investigate the difference between the measured and predicted sensitivity enhancements.

5. Conclusions

This study demonstrates the possibility of employing the low temperature post-CMOS process inherited from the mature pick-and-place technology for packaging to easily improve the performance of CMOS MEMS devices. Thus, a CMOS MEMS capacitive type 2-axis tilt sensor with a bonded bulk solder ball and the monolithic integrated sensing circuits has been successfully designed and implemented. The suspended structure is fabricated based on the standard TSMC $0.35\ \mu\text{m}$ 2P4M process and the post-CMOS etching process. The

$95\ \mu\text{m}$ solder ball is bonded to the suspended stage using the low temperature UV-glue dispensing and curing processes. The sensitivity of the 2-axis tilt sensor has been increased for 2.06-fold in x -axis and 1.78-fold in y -axis after adding the solder ball. Due to the out-of-plane offset of sensing electrodes and the existing of parasitic capacitance for solder ball, the measured sensitivity is smaller than the one predicted from analysis. Thus, the sensitivity can be further improved by reducing the parasitic capacitance and the mismatch of sensing electrodes caused by solder ball. In addition, the low temperature pick-and-place technology can be further extended to assemble various micro scale objects onto MEMS structures for different applications.

Acknowledgments

This study is sponsored in part by the National Science Council of Taiwan under grant of NSC-102-2218-E-007-003. The authors would like to appreciate support from the TSMC and the National Chip Implementation Center (CIC), Taiwan, for CMOS chip manufacturing. The authors wish to thank the Center for Nanotechnology, Material Science, and Microsystem of National Tsing Hua University and the National Nano Device Laboratory in providing fabrication facilities. The authors would also like to thank the National Center for High-Performance Computing for the supporting of simulation tools.

References

- [1] Song C and Shinn M 1998 Commercial vision of silicon-based inertial sensors *Sensors Actuators A* **66** 231–6
- [2] Jung H, Kim C J and Kong S H 2007 An optimized MEMS-based electrolytic tilt sensor *Sensors Actuators A* **139** 23–30
- [3] Chen S J and Shen C H 2008 A novel two-axis CMOS accelerometer based on thermal convection *IEEE Trans. Instrum. Meas.* **57** 1572–7
- [4] Milanovic V, Bowen E, Zaghoul M E, Tea N H, Suehle J S, Payne B and Gaitan M 2000 Micromachined convective accelerometers in standard integrated circuits technology *Appl. Phys. Lett.* **76** 508–10
- [5] Billat S, Glosch H, Kunze M, Hedrich F, Frech J, Auber J, Sandmaier H, Wimmer W and Lang W 2002 Micromachined inclinometer with high sensitivity and very good stability *Sensors Actuators A* **97–98** 125–30
- [6] Lin C S and Kuo S M 2007 High-performance inclinometer with wide-angle measurement capability without damping effect *Proc. 20th IEEE Int. Conf. on Micro Electro Mechanical Systems, (Kobe, Japan, Jan.)* pp 585–8
- [7] Liu T, Sen P and Kim C J 2012 Characterization of nontoxic liquid-metal alloy galinstan for applications in microdevices *J. Microelectromech. Syst.* **21** 443–50
- [8] Yun S-S, Jeong D H, Wang S M, Je C H, Lee M L, Hwang G, Choi C A and Lee J H 2009 Fabrication of morphological defect-free vertical electrodes using a (1 1 0) silicon-on-patterned-insulator process for micromachined capacitive inclinometers *J. Micromech. Microeng.* **19** 035025

- [9] Liang J, Kohsaka F, Li X, Kunitomo K and Ueda T 2009 Characterization of a quartz MEMS tilt sensor with 0.001° precision *Proc. 15th Int. Conf. on Solid-State Sensors, Actuators and Microsystems, (Denver, CO, June)* pp 308–10
- [10] Xie H, Erdmann L, Zhu X, Gabriel K and Fedder G K 2002 Post-CMOS processing for high-aspect-ratio integrated silicon microstructures *J. Microelectromech. Syst.* **11** 93–101
- [11] Hierlemann A, Brand O, Hagleitner C and Baltes H 2003 Microfabrication techniques for chemical/biosensors *Proc. IEEE* **91** 839–63
- [12] Neumann J J Jr and Gabriel K J 2002 CMOS-MEMS membrane for audio-frequency acoustic actuation *Sensors Actuators A* **95** 175–82
- [13] Chavan A V and Wise K D 2002 A monolithic fully-integrated vacuum-sealed CMOS pressure sensor *IEEE Trans. Electron Devices* **49** 164–9
- [14] Zhang G, Xie H, de Rosset L E and Fedder G K 2008 A lateral capacitive CMOS accelerometer with structural curl compensation *Proc. 21st IEEE Int. Conf. on Micro Electro Mechanical Systems, (Orlando, FL, Jan.)* pp 606–11
- [15] Sun C-M, Wang C and Fang W 2008 On the sensitivity improvement of CMOS capacitive accelerometer *Sensors Actuators A* **141** 347–52
- [16] Tsai M-H, Sun C-M, Liu Y-C, Wang C and Fang W 2009 Design and fabrication of a metal wet-etching post-process for the improvement of CMOS-MEMS capacitive sensors *J. Micromech. Microeng.* **19** 105017
- [17] Qu H and Xie H 2007 Process development for CMOS-MEMS sensors with robust electrically isolated bulk silicon microstructures *J. Microelectromech. Syst.* **16** 1152–61
- [18] Liu Y-C, Tsai M-H, Tang T-L and Fang W 2011 Post-CMOS selective electroplating technique for the improvement of CMOS-MEMS accelerometers *J. Micromech. Microeng.* **21** 105005
- [19] Tsui K, Geisberger A A, Ellis M and Skidmore G H 2004 Micromachined end-effector and techniques for directed MEMS assembly *J. Micromech. Microeng.* **14** 542–9
- [20] Kim C, Pisano A P, Muller R S and Lin M G 1992 Polysilicon microgripper *Sensors Actuators A* **33** 221–7
- [21] Carrozza M C, Menciassi A, Tiezzi G and Dario P 1998 The development of a LIGA-microfabricated gripper for micromanipulation tasks *J. Micromech. Microeng.* **8** 141–3
- [22] Chang C-I, Tsai M-H, Liu Y-C, Sun C-M and Fang W 2011 Design and implementation of an extremely large proof-mass CMOS-MEMS capacitive tilt sensor for sensitivity and resolution improvement *Proc. 16th Int. Conf. on Solid-State Sensors, Actuators and Microsystems, (Beijing, China, June, 2011)* pp 1104–7
- [23] Sun C-M, Tsai M-H, Liu Y-C and Fang W 2010 Implementation of a monolithic single proof-mass tri-axis accelerometer using CMOS-MEMS technique *IEEE Trans. Electron Devices* **57** 1670–9